Structure of Zip2:Spo16, a conserved XPF:ERCC1-like complex critical for meiotic crossover formation

Kanika Arora[1], Kevin D. Corbett[1,2,3,*]

[1] Ludwig Institute for Cancer Research, San Diego Branch

[2] Department of Chemistry and Biochemistry, University of California, San Diego

[3] Department of Cellular and Molecular Medicine, University of California, San Diego, La Jolla, CA 92093, USA

* To whom correspondence should be addressed: kcorbett@ucsd.edu

Running title: Structure of Zip2:Spo16 complex

Abstract

In eukaryotic meiosis, generation of haploid gametes depends on the formation of inter-homolog crossovers, which enable homolog segregation to reduce ploidy in the meiosis I division. A class of conserved meiosis-specific proteins, collectively termed ZMMs, are required for formation and spatial control of crossovers throughout eukaryotes. Here, we show that three *S. cerevisiae* ZMM proteins – Zip2, Zip4, and Spo16 – interact with one another to form a complex critical for crossover formation and control. We reconstituted and determined the crystal structure of a Zip2:Spo16 subcomplex, revealing a heterodimer structurally related to the XPF:ERCC1 endonuclease complex. We show that Zip2:Spo16 binds specific DNA structures found in early meiotic recombination intermediates, but does not possess and intact endonuclease site. Overall, our data support a model in which Zip2:Spo16 binds and stabilizes early meiotic recombination intermediates, while the associated TPR protein Zip4 recruits additional factors to promote crossover formation and license synaptonemal complex assembly. Given the recent identification of Zip2 homologs outside fungi, the molecular mechanisms we outline are likely conserved throughout eukaryotes.

Keywords

Crossover interference / Meiotic recombination / XPF-ERCC1 / ZMM proteins

Introduction

Sexual reproduction in eukaryotes entails the production of haploid gametes through a specialized cell-division program called meiosis, followed by the fusion of two gametes to generate diploid offspring. The reduction of ploidy in meiosis is enabled by the formation of crossovers or chiasmata, specific inter-homolog recombination events that physically link homologs and enable their segregation in the meiosis I division. Because of their importance for accurate chromosome segregation, the formation of most crossovers (COs) is subject to tight spatial and temporal regulation: overlapping feedback pathways ensure that while each homolog pair receives at least one CO, the overall number of COs is kept within a tight range and no two COs are positioned too close to one another along the chromosome (reviewed in (Wang *et al*, 2015; Berchowitz & Copenhaver, 2010)). Defects in the production or spatial regulation of COs can lead to aneuploidy in offspring, a major cause of miscarriage and developmental disorders in humans (Hassold *et al*, 2007; Hassold & Hunt, 2001).

While the molecular machinery driving CO formation is highly conserved, the budding yeast *S. cerevisiae* has served as the primary experimental system for understanding how CO formation is controlled. In *S. cerevisiae*, as in other organisms, entry into meiotic prophase is accompanied by assembly of the meiotic chromosome axis, which organizes each pair of replicated sister chromosomes as a linear array of chromatin loops. The chromosome axis proteins Hop1 and Red1 promotes the formation of DNA double-strand breaks (DSBs) along each chromosome by the Spo11 endonuclease. These DSBs are resected to free 3' single-stranded ends and loaded with two related recombinases, Rad51 and Dmc1, which mediate the invasion of a homologous DNA duplex to form a so-called D-loop intermediate (Bishop *et al*, 1992; Cloud *et al*, 2012). In meiotic prophase, use of the identical sister chromatid as a repair template is strongly inhibited by the chromosome axis, thereby promoting invasion of the homolog instead (Niu *et al*, 2005; Subramanian *et al*, 2016; Carballo *et al*, 2008; Niu *et al*, 2009; 2007; Schwacha & Kleckner, 1997). After initial invasion of the homolog and formation of a D-loop, several competing pathways vie to determine the fate of the intermediate. Often, the D-loop is dissolved by the combined action of DNA topoisomerases and helicases (in *S. cerevisiae*, the Sgs1,Top3, and Rmi1 proteins) [13-15]. If the free 3' end has undergone new DNA synthesis past the original break, it may re-anneal with the other broken end to give a non-crossover (NCO); this pathway is referred to as synthesis-dependent strand annealing (SDSA) and is responsible for the bulk of NCO formation. A subset of strand invasion intermediates are further processed into double Holliday Junction (dHJ) intermediates (Hunter & Kleckner, 2001; Schwacha & Kleckner, 1995), which may become either COs or NCOs. Type 1 "interfering" COs are generated by specific cleavage of dHJs by the Mlh1:Mlh3 endonuclease (Zakharyevich *et al*, 2012). A minor competing

pathway involving non-specific endonucleases (in *S. cerevisiae*, Mus81:Mms4, Yen1, and Slx1:Slx4) can generate either NCOs or type 2 "noninterfering" COs (De Muyt *et al*, 2012).

The formation of type 1 COs is tightly regulated by a group of proteins collectively termed "ZMM" proteins: Zips (Zip1/Zip2/Zip3/Zip4), Msh4:Msh5, and Mer3 (Lynn *et al*, 2007). These proteins play a variety of roles in CO formation, notably including the stabilization of early recombination intermediates against dissolution by topoisomerases/helicases, and coupling recombination to assembly of the synaptonemal complex. This conserved ladder-like structure assembles processively from initial homolog interaction sites including centromeres and recombination sites, and brings homologs into close juxtaposition along their lengths. Synaptonemal complex assembly is also coordinated with removal of Hop1 from the axis by the AAA+ ATPase Pch2 (Chen *et al*, 2014; Joshi *et al*, 2009; Borner *et al*, 2008), with the loss of Hop1 suppressing further DSB and CO formation.

Most ZMM proteins are conserved throughout eukaryotes, and their roles in promoting CO formation are generally well-outlined: for example, Mer3 is a DNA helicase (Mazina *et al*, 2004) and Msh4:Msh5, relatives of the MutS family DNA mismatch recognition proteins, are proposed to bind and stabilize a branched recombination intermediate and recruit the Mlh1:Mlh3 endonuclease for specific dHJ cleavage (Snowden *et al*, 2008; 2004). Zip3 is related to ubiquitin/SUMO E3 ligase proteins (Perry *et al*, 2005), and as such likely has a role in regulation of protein complex formation or degradation at crossover sites (Ahuja *et al*, 2017; Rao *et al*, 2017). Zip1 is the major component of "transverse filaments" within the synaptonemal complex, a conserved structure that links homologs and is important for the resolution of crossovers (Zickler & Kleckner, 1999; Sym *et al*, 1993; Dong & Roeder, 2000).

Of the identified ZMM proteins in *S. cerevisiae*, the roles of Zip2, Zip4, and their more recently-identified binding partner Spo16 are the least well-understood. These three proteins localize to recombination sites on meiotic chromosomes (Fung *et al*, 2004; Chua & Roeder, 1998) and depend on one another for localization (Tsubouchi *et al*, 2006; Shinohara *et al*, 2008), suggesting that they act together as a complex. All three proteins are required for wild-type levels of COs (Chua & Roeder, 1998; Shinohara *et al*, 2008; Malavasic & Elder, 1990; Tsubouchi *et al*, 2006), *zip2* and *zip4* mutants show defects in crossover interference (Tsubouchi *et al*, 2006; Chen *et al*, 2008), and *zip2* mutants also show a dramatic reduction in single-end invasion and dHJ recombination intermediates (Börner *et al*, 2004). Together, these data suggest that Zip2, Zip4, and Spo16 may directly promote the formation of type I COs, potentially by aiding the formation of early recombination intermediates, or stabilizing these intermediates against disassembly. In addition to their effects on meiotic recombination, these proteins also play a key role in synaptonemal complex assembly: in *zip2*, *zip4*, and *spo16* mutants, Zip1 forms foci at recombination sites, but does not

extend along chromosomes to form the full synaptonemal complex [33-35]. Zip2 and Zip4 have also been observed to localize at the ends of Zip1 stretches, both on synapsed chromosomes and on extra-chromosomal Zip1 assemblies termed polycomplexes (Tsubouchi *et al*, 2006; Chua & Roeder, 1998). These findings suggest that Zip2, Zip4, and Spo16 directly interact with Zip1 or other synaptonemal complex proteins, and play a direct role in coordinating CO formation with assembly of the synaptonemal complex.

Sequence analyses and 3D structure predictions have revealed that *S. cerevisiae* Zip2 and its *Arabidopsis thaliana* homolog SHOC1 show distant homology to XPF, a structure-specific endonuclease that plays important roles in nucleotide excision repair with its binding partner, ERCC1 (Macaisne *et al*, 2011; 2008). *A. thaliana* SHOC1 forms a complex with a second protein, PTD (Macaisne *et al*, 2011), suggesting that an XPF:ERCC1-like complex may play a conserved role in meiotic CO formation across eukaryotes. Here, we outline the architecture of the Zip2:Zip4:Spo16 complex and show by x-ray crystallography that Zip2 and Spo16 form an XPF:ERCC1-like heterodimer. Zip2 lacks an endonuclease active site, suggesting that Zip2:Spo16 acts not as an endonuclease, but instead as a structure-specific DNA binding factor. We show that, like XPF:ERCC1, Zip2:Spo16 can bind a variety of DNA structures, including single-strand/double-strand DNA junctions with the geometry found in meiotic strand-invasion intermediates. We propose a model in which the Zip2:Zip4:Spo16 complex cooperates with Msh4:Msh5 to recognize and stabilize early recombination intermediates, recruit downstream crossover factors to promote the formation of type I COs, and coordinate the formation of COs with assembly of the synaptonemal complex.

Results & Discussion

Architecture of the Zip2:Spo16:Zip4 complex

Zip2, Spo16, and Zip4 share similar roles in promoting meiotic crossover formation and synaptonemal complex assembly, co-localize on meiotic chromosomes, and depend on one another for their chromosome localization (Tsubouchi *et al*, 2006; Shinohara *et al*, 2008). Aside from one report of co-immunoprecipitation of Spo16 and Zip4 (Shinohara *et al*, 2008), however, whether and how these proteins directly interact is unknown. To comprehensively outline interactions between Zip2, Spo16, and Zip4, we used yeast two-hybrid analysis. We found that Spo16 interacts strongly with a truncated construct of Zip2 (residues 499-704) containing this protein's putative XPF-like domain (full-length Zip2 showed autoactivation in these assays, and could not be tested) (**Figure 1A,B**). We also found that Zip2's N-terminal region (residues 1-499) interacts with full-length Zip4, though this interaction was only detected with one tag configuration (**Figure 1B**). Given that the Zip2 C-terminal region interacts with Spo16, we reasoned that full-length Zip2 may depend on Spo16 for solubility. Thus, we next performed yeast three-hybrid assays with one vector encoding both Zip2 and Spo16, and a second vector encoding Zip4. We found that while Zip2:Spo16 strongly interacts with Zip4, removing the Zip2 N-terminal domain (residues 1-498) disrupts this interaction (**Figure 1C**). Together, these data strongly indicate that the Zip2 C-terminal domain forms a complex with Spo16, and the Zip2 N-terminal domain likely interacts with Zip4. Efforts to truncate Zip4 to identify the Zip2-binding region were unsuccessful, perhaps due to structural disruptions from truncating the protein's array of TPR repeats (not shown).

The Zip2:Spo16 structure reveals an XPF:ERCC1-like complex

We next co-expressed Zip2 and Spo16 in *E. coli* for structural and biochemical analysis. While full-length Zip2 expressed poorly and was mostly insoluble, even when coexpressed with Spo16, we could co-express and purify the Zip2 XPF-like domain (residues 499-704; Zip2$^{499\text{-}704}$) with Spo16. The Zip2$^{499\text{-}704}$:Spo16 complex forms a well-behaved 1:1 heterodimer (**Figure 1D,E**). While initial crystallization efforts were unsuccessful, we obtained crystals of the complex after methylation of surface lysine residues by formaldehyde/dimethylamine borane complex treatment (**Figure S1A**) (Walter *et al*, 2006; Kim *et al*, 2008). The resulting crystals (termed Form 1 hereon) adopted space group C2 and contained four copies of the complex per asymmetric unit. Extensive efforts to determine the structure of Form 1 crystals using heavy-atom derivatives failed, due to translational pseudo-symmetry in these crystals.

To identify additional crystal forms for the Zip2$^{499\text{-}704}$:Spo16 complex, we turned to surface entropy reduction. We mutated the highest-scoring segment in Zip2 identified by the UCLA SERp Server (Goldschmidt *et al*, 2007), residues 641-643, from the sequence KEK to AAA. The mutated complex,

Zip2$^{499-704}$SER:Spo16, behaved equivalently to wild-type protein and crystallized in several new conditions without surface lysine methylation. We optimized one condition in space group $P2_12_12_1$ (termed Form 2 hereon), which contained one copy of the Zip2$^{499-704}$SER:Spo16 complex per asymmetric unit. We determined the structure of Form 2 crystals by single-wavelength anomalous diffraction methods using a 2.38 Å-resolution dataset collected from a crystal grown from selenomethionine-derivatized protein (**Figure 2A**). We then used molecular replacement to determine the Form 1 structure, resulting in a total of five crystallographically-independent views of the Zip2$^{499-704}$:Spo16 complex. The structures of Form 1 and Form 2 are highly similar (overall Cα r.m.s.d. 0.3-1.4 Å; **Figure S2**), indicating that neither surface lysine methylation nor surface entropy reduction significantly alters the complex's structure.

The overall structure of Zip2$^{499-704}$:Spo16 is quite similar to known XPF:ERCC1 and related complexes (**Figure 2A**). Zip2 possesses an XPF-like central domain (residues 499-640) and a C-terminal tandem helix-hairpin-helix (HhH_2) domain (residues 641-704). The Zip2 residues we mutated for surface entropy reduction, 641-643, are located on the inter-domain linker and are disordered in the Form 2 crystals. Spo16 shows a similar two-domain structure, with an N-terminal central domain similar in fold to ERCC1, though significantly diverged (**Figure S3**). Unlike the tandem HhH motifs found in the ERCC1 C-terminus, the Spo16 C-terminal domain contains only a single HhH motif (**Figure 2B, S3**). The Zip2 and Spo16 central domains form a tight pseudo-symmetric dimer, with flexible linkers connecting these domains to the C-terminal HhH domains, which also form a tight dimer. The conformations of the linker regions and the relative positions of the central and HhH domains are highly similar in the five independent views of the Zip2$^{499-704}$:Spo16 complex, suggesting that the complex is relatively rigid (**Figure S2**). The juxtaposition of central and C-terminal domains is also similar to a recent structure of the human FANCM:FAAP24 complex, an inactive XPF:ERCC1-like complex with a key role in the Fanconi Anemia (FA) "core" DNA-repair complex (Yang *et al*, 2013).

The key biochemical activities of XPF:ERCC1 are structure-specific DNA binding and single-strand DNA cleavage, primarily at single-strand:double-strand DNA junctions, as part of its role in the nucleotide excision repair pathway (Ciccia *et al*, 2008). DNA cleavage is accomplished by a highly-conserved active site on the XPF central/nuclease domain. To learn whether Zip2 may share this activity, we overlaid the Zip2 central domain with the structure of *Aeropyrum pernix* XPF nuclease domain (Newman *et al*, 2005), and examined the region around the XPF active site. The XPF active site is characterized by several highly-conserved residues, including a conserved aspartate residue (D52 in *Ap* XPF) and E-R-K motif (residues 62-64 in *Ap* XPF), with the aspartate and glutamate residues coordinating a critical Mg^{2+} ion cofactor (**Figure 2D**). In Zip2, the conserved aspartate in the XPF active site is indeed an aspartate (D538) that is highly conserved among budding-yeast Zip2 proteins (replaced by a histidine residue in *C. glabrata* Zip2).

The residues corresponding to the XPF E-R-K motif, however, are not well-conserved: *S. cerevisiae* Zip2 possesses tyrosine, lysine, and isoleucine, respectively, in these positions (residues 548-550). These residues are poorly conserved among Zip2 orthologs. In addition, when we determined a structure from crystals grown in the presence of 10 mM $MgCl_2$, we saw no evidence of a bound Mg^{2+} ion in this site (data not shown). Thus, despite the conservation of one key active site residue with XPF, our structural evidence overall points to Zip2 lacking endonuclease activity. This finding is again reminiscent of the FANCM:FAAP24 complex, of which the XPF ortholog FANCM also lacks endonuclease activity. Since FANCM:FAAP24 is thought to bind specific DNA structures and scaffold the assembly of a multi-subunit DNA repair complex (Yang *et al*, 2013), a similar DNA binding/scaffolding activity could explain existing genetic data on the roles of *ZIP2* and *SPO16* in CO formation.

Zip2:Spo16 binds a range of DNA structures

To test whether Zip2:Spo16 complex can bind specific DNA structures, we performed quantitative electrophoretic mobility-shift assays with reconstituted $Zip2^{499-704}$:Spo16 complex and specific DNA structures with elements of early meiotic recombination intermediates. We tested binding of $Zip2^{499-704}$:Spo16 first to single-stranded DNA (ssDNA) and double-stranded (dsDNA) duplexes 40 base pairs in length, and found robust binding to dsDNA (**Figure 3A**) but barely-detectable association with ssDNA (**Figure S4A**). We next tested binding to ssDNA-dsDNA junction substrates as the initial strand invasion event will generate a D-loop intermediate with a ssDNA-dsDNA junction with a 5' overhang. We tested binding of $Zip2^{499-704}$:Spo16 to junctions of both polarity and observed robust binding to both (**Figure 3B, C**), though binding to the 5'-overhang substrate appeared more robust. Finally, we tested binding of a Holliday Junction (HJ) substrate with 20-bp arms. While Zip2:Zip4:Spo16 localizes to meiotic recombination sites prior to the formation of the double Holliday Junction intermediate, binding to this substrate could indicate specificity for other DNA structures formed prior to the double Holliday Junction. Indeed, we observed significantly stronger binding of $Zip2^{499-704}$:Spo16 to the HJ substrate than to either dsDNA or the 5'-overhang substrate (**Figure 3D**). We also observed multiple shifted bands on our gels with the HJ substrate, indicating that multiple $Zip2^{499-704}$:Spo16 complexes likely bind a single HJ at high protein concentrations. Overall these data show that $Zip2^{499-704}$:Spo16 robustly binds multiple DNA structures potentially found in early meiotic recombination intermediates.

Examination of the surface of $Zip2^{499-704}$:Spo16 revealed a large positively-charged surface on Zip2, at the interface between this subunit's central domain and HhH_2 domain (**Figure 3E**). This surface corresponds to a surface of the *H. sapiens* XPF HhH_2 domain observed o bind single-stranded DNA in a prior NMR structure (Das *et al*, 2012), supporting its potential role in DNA binding in the Zip2:Spo16 complex.

Based on this finding, we generated two mutant complexes, the first (mutant #1) with K663, K683, and K686 on the Zip2 HhH_2 domain mutated to alanine, and the second (mutant #2) with these mutations plus K609A on the Zip2 central domain (**Figure 3F**). These mutations did not affect the expression, solubility, or stability of $Zip2^{499-704}$:Spo16 complex (**Figure S4B, C**). We tested binding of both mutants to the 5'-overhang and Holliday Junction substrates, and found that both were significantly compromised in DNA binding (**Figure 3G, H**). While mutant #1 showed some residual binding to the 5' overhang substrate, mutant #2 showed no detectable binding. Both mutants bound very weakly to the Holliday Junction substrate, but did not show the multiple shifted bands we observed with wild-type complex. Thus, $Zip2^{499-704}$:Spo16 binds DNA through a large positively-charged surface comprising the Zip2 HhH_2 and central domains. The primary role of Zip2, and not Spo16, in DNA binding may explain why Spo16 is so highly diverged from ERCC1 and its relatives.

The role of Zip2:Spo16:Zip4 in meiotic crossover control

The data we present here indicates that the *S. cerevisiae* Zip2:Spo16 complex forms an XPF:ERCC1-like dimer that lacks an endonuclease active site, but likely possesses structure-specific DNA binding activity. We further show that the Zip2 N-terminal domain binds Zip4 to scaffold the assembly of a larger Zip2:Spo16:Zip4 complex. Based on prior work, the Zip2:Spo16:Zip4 complex is required for formation of type I COs in yeast, and also is required for polymerization of the synaptonemal complex in coordination with crossover formation. Based on its structure and DNA binding activity, we propose that Zip2:Spo16 binds a specific DNA structure generated early in the recombination pathway, perhaps the ssDNA-dsDNA junction with a 5' single-strand overhang formed after strand invasion and initial synthesis (**Figure 4A,B**). By binding this intermediate, Zip2:Spo16 could complement the activity of the Msh4:Msh5 complex, which is proposed to bind a pre-Holliday Junction intermediate. Thus, Zip2:Spo16 and Msh4:Msh5 could together recognize and stabilize multiple structural elements of an recombination intermediate, thereby stabilizing this intermediate against dissolution by topoisomerases/helicases to promote the crossover fate (**Figure 4C**).

In addition to promoting and stabilizing early recombination intermediates, Zip2:Zip4:Spo16 is also important for assembly of the synaptonemal complex, likely linking events at the DNA level with a "licensing" of synaptonemal complex assembly once recombination has progressed to a certain point. We propose that, similar to the role of FANCM:FAAP24 in the FA core complex, Zip2:Spo16:Zip4 can recruit and organize different proteins, to promote the crossover fate and synaptonemal complex assembly. This recruitment is likely accomplished mostly by Zip4, which is large (975 amino acids) and predicted to fold into an array of 22 TPR repeats ((Perry *et al*, 2005) and our own analysis). In addition to

Zip4, close inspection of our Zip2$^{499-704}$:Spo16 complex reveals a conserved, concave hydrophobic surface involving the C-terminal W704 residue of Zip2 and two α-helices from the Spo16 HhH domain (**Figure S5**). This interface binds a short hydrophobic α-helix on the Zip2 central domain in three of the five crystallographically-independent views of the complex (two of the four copies in Form 1, plus the single copy from Form 2), burying 410 Å^2 of mostly-hydrophobic surface area on each partner. Based on the high conservation of the involved residues on the Spo16 HhH domain, their mostly hydrophobic nature, and our observation of this interface in both crystal forms of Zip2$^{499-704}$:Spo16, we propose that this surface may be involved in specific protein-protein interactions. While our initial yeast two-hybrid assays revealed no interactions between Zip2:Spo16 and other known ZMM/chromosome axis/synaptonemal complex proteins, the role of this surface will be an interesting avenue for future work, especially given the likelihood that Zip2:Zip4:Spo16 acts a scaffolding complex for DNA repair and synaptonemal complex assembly.

In *A. thaliana*, SHOC1 and PTD interact with one another and are required for the formation of type I COs, and sequence analyses have suggested that these proteins also form an XPF:ERCC1-like dimer (Macaisne *et al*, 2011; 2008). Further sequence analysis also identified a potential human SHOC1 ortholog, C9orf84, indicating that an XPF:ERCC1-like complex might be a conserved feature of meiosis in eukaryotes (Macaisne *et al*, 2011). Further work will be required to identify how these complexes cooperate with the conserved Msh4:Msh5 complex and recruit downstream recombination factors to promote the crossover fate, and how this complex coordinates events at the DNA level with chromosome morphological changes such as synaptonemal complex assembly.

Materials & Methods

Yeast two-hybrid assays

For yeast two-hybrid assays, individual proteins were cloned into pBridge and pGADT7 AD vectors (Clontech) with multiple-cloning sites modified for ligation-independent cloning (http://qb3.berkeley.edu/macrolab/lic-cloning-protocol/). pBridge vectors were transformed into *S. cerevisiae* strain AH109 and selected on SC media lacking tryptophan (-TRP). pGADT7 AD vectors were transformed into *S. cerevisiae* strain Y187 and selected on SC media lacking leucine (-LEU). Haploid strains were mated and diploids selected on SC -TRP/-LEU. Diploid cells were diluted in water and replated onto SC -TRP/-LEU (control), -TRP/-LEU/-HIS (histidine) (low stringency), and -TRP/-LEU/-HIS/-ADE (adenine) (high stringency), grown for 2-3 days, then examined for growth.

For yeast three-hybrid assays, pBridge vectors containing either Spo16 or Zip2 in MCS I were further modified by NotI cleavage at the MCS II site followed by isothermal assembly-mediated insertion of the second gene (Gibson *et al*, 2009), resulting in a single vector encoding a Zip2:Spo16 complex containing the Gal4-BD tag fused to the N-terminus of either protein. These vectors were transformed into AH109 and mated with pGADT7 AD vectors encoding Zip4.

Protein expression and purification

Ligation-independent cloning was used to clone full length Spo16 and Zip2$^{499\text{-}704}$. To express TEV protease-cleavable, His_6-tagged Spo16, full-length Spo16 was cloned into Addgene vector 48324 (contains Spectinomycin resistance and CloDF13 ori) using ligation-independent cloning. To express untagged Zip2 499-704, DNA encoding Zip2 499-704 was cloned into Addgene vector 29665 (contains Ampicillin resistance and ColE1 origin of replication) using ligation-independent cloning. The Zip2 surface entropy reduction (SER) mutant (KEK 641-643 → AAA) was identified by the UCLA SERp server (http://services.mbi.ucla.edu/SER/) (Goldschmidt *et al*, 2007) and was generated by mutagenic PCR.

For protein expression, plasmids encoding Zip2$^{499\text{-}704}$ (unmutated or SER mutant) and full-length Spo16 were co-transformed into *E. coli* Rosetta2 (DE3) pLysS cells, and grown in 2XYT media supplemented with both ampicillin and spectinomycin. Cells were grown at 37°C to and OD_{600} of 0.6, shifted to 20°C and protein expression induced with 0.25 mM IPTG, and grown 16 hours. For selenomethionine derivatization, cells were grown in M9 minimal media at 37°C to an OD_{600} of 0.8, after which the following amino acids were added: Leu, Ile and Val (50 mg/L), Phe, Lys, Thr (100 mg/L) and Selenomethionine (60 mg/L). Cells were shifted to 20°C and protein expression was induced with 0.25 mM IPTG after 20 minutes incubation with amino acids.

For protein purification, cells were harvested by centrifugation, suspended in resuspension buffer (20 mM Tris-HCl pH 8.0, 300 mM NaCl, 10 mM imidazole, 1 mM dithiothreitol (DTT) and 10% glycerol) and lysed by sonication. Lysate was clarified by centrifugation (16,000 rpm 30 min), then supernatant was loaded onto a Ni^{2+} affinity column (HisTrap HP, GE Life Sciences) pre-equilibrated with resuspension buffer. The column was washed with buffer containing 20 mM imidazole and 100 mM NaCl, and eluted with a buffer containing 250 mM imidazole and 100 mM NaCl. The elution was loaded onto an anion-exchange column (Hitrap Q HP, GE Life Sciences) and eluted using a 100-600 mM NaCl gradient. Fractions containing the protein were pooled and concentrated to 2 mL by ultrafiltration (Amicon Ultra-15, EMD Millipore), then passed over a size exclusion column (HiLoad Superdex 200 PG, GE Life Sciences) in a buffer containing 20 mM Tris-HCl pH 8.0, 200 mM NaCl, and 1 mM DTT. For His_6-tag cleavage, anion-exchange elution fractions were pooled and mixed with purified TEV protease (20:1 weight-weight ratio) and incubated 24-48 hours at 4°C. The mixture was passed over a Ni^{2+} affinity column to bind uncleaved protein, cleaved His_6-tags, and His_6-tagged TEV protease, then flow-through fractions were pooled, concentrated, and purified by size-exclusion as above. Purified proteins were concentrated by ultrafiltration and stored at 4°C for crystallization, or aliquoted and frozen at -80°C for biochemical assays.

Surface lysine residues were dimethylated by incubating the protein with 20 mM freshly-prepared Dimethylamine Borane Complex and 40 mM formaldehyde, incubated at 4°C for one hour, then the reaction was stopped by addition of 100 mM glycine. Alkylated proteins were purified by size-exclusion chromatography as above. Dimethyl-lysine residues can be observed in several positions in electron density maps of Form 1 crystals (**Figure S1A, B**).

For size exclusion chromatography coupled to multi-angle light scattering (SEC-MALS), 100 µL of $Zip2^{499-704}$:His_6-Spo16 at 2.0 mg/mL was injected onto a Superdex 200 Increase 10/300 GL column (GE Life Sciences) in a buffer containing 20 mM HEPES pH 7.5, 300 mM NaCl, 5% glycerol, and 1 mM DTT. Light scattering and refractive index profiles were collected by miniDAWN TREOS and Optilab T-rEX detectors (Wyatt Technology), respectively, and molecular weight was calculated using ASTRA v. 6 software (Wyatt Technology).

For measurement of melting temperature, 45 uL 0.1 mg/mL purified protein in gel-filtration buffer was mixed with 5 µL 50X SYPRO orange dye (Life Technologies; 5X final concentration) and pipetted into an optically-clear qPCR plate. SYPRO fluorescence was measured in a Bio-Rad CFX96 qPCR machine in FRET mode (excitation 450-490 nm, emission 560-580) using a temperature range 25-95°C in 0.5° steps (15 second hold per step). Triplicate measurements were averaged, buffer-subtracted, then the derivative

of the fluorescence was calculated. The maximum value of the derivative curve (highest rate of change in fluorescence) is assigned as the melting temperature.

Protein crystallization

Form 1 crystals were obtained in hanging drops with surface-lysine methylated His_6-tagged $Zip2^{499-704}$:Spo16 at 10 mg/mL in a buffer containing 20 mM Tris-HCl pH 7.5 and 200 mM NaCl. Protein was mixed 1:1 with well solution containing 1.4 M Na-K phosphate pH 6.6. Crystals were transferred to a cryoprotectant solution containing 2.4 M Na malonate pH 7, then flash-frozen in liquid nitrogen. Form 2 crystals were obtained in hanging drops with $Zip2^{499-704}$SER:Spo16 at 10 mg/mL in a buffer containing 20 mM Tris-HCl pH 7.5 and 200 mM NaCl. Protein was mixed 1:1 with well solution containing 100 mM Bis Tris pH 5.5, 200 mM Ammonium sulfate, 15% PEG-3350. Crystals were cryo-protected by addition of 15-20% PEG-400, then flash-frozen in liquid nitrogen.

X-Ray data collection and structure determination

For Form 1, diffraction data was collected at the Advanced Photon Source, NE-CAT beamline 24ID-E (support statement below). Data was automatically indexed and reduced by the RAPD data-processing pipeline (https://github.com/RAPD/RAPD). Extensive efforts to determine the structure by anomalous methods using selenomethionine-derivatized protein failed due to translational pseudo-symmetry arising from the positions and orientations of the four copies of $Zip2^{499-704}$:Spo16 in these crystals.

For Form 2, diffraction data for both native and selenomethionine-derivatized crystals were collected at the Advanced Photon Source, NE-CAT beamline 24ID-C, and data was automatically indexed and reduced by the RAPD data-processing pipeline, which uses XDS (Kabsch, 2010) for indexing and integration, and the CCP4 programs AIMLESS and TRUNCATE (Winn *et al*, 2011) for scaling and structure-factor calculation. The structure was determined by single-wavelength anomalous diffraction (SAD) methods using a 2.38 Å-resolution dataset collected from selenomethionine-derivatized proteins. Selenium sites were located using hkl2map/SHELX (Pape *et al*, 2004; Sheldrick, 2010), and provided to the Phenix Autosol pipeline (Terwilliger *et al*, 2009; Adams *et al*, 2010) for phase calculation using PHASER (McCoy *et al*, 2007) and density modification using RESOLVE (Terwilliger, 2000). A partial model built by RESOLVE (Terwilliger, 2003) was manually rebuilt in COOT (Emsley *et al*, 2010) and refined against a 2.13 Å-resolution native dataset using phenix.refine (Afonine *et al*, 2012).

To determine the Form 1 structure, molecular replacement was performed using PHASER to place four copies of the Form 1 dimer structure. The model was manually rebuilt in COOT and refined in phenix.refine to 2.29 Å resolution. Refined electron-density maps revealed additional electron density

extending the side-chain of Zip2 Cys521 in all four copies of the complex. Formaldehyde, which was used for surface lysine alkylation of the complex, can react with the cysteine side-chain to produce hydroxymethylcysteine (Bateman *et al*, 2007; Metz *et al*, 2004), which closely matches the observed electron density for this residue (**Figure S1C,D**). We also observed clear electron density for several residues in the N-terminal His_6-tag fused to Spo16, which included a TEV protease cleavage site (MKSSHHHHHHENLYFQ^SNA-[$Spo16^{2-198}$]), packing against a symmetry-related copy of Spo16, explaining why these crystals required an intact tag for growth (**Figure S1E**). Data collection and refinement statistics for both structures can be found in **Table S1**. All structure figures were created with PyMOL version 2, and surface charge calculations were performed with the APBS (Jurrus *et al*, 2018) plugin in PyMOL.

Electrophoretic mobility shift assays

To generate different DNA substrates for electrophoretic mobility shift assays, a 40-base oligonucleotide 5'-labeled with 6-carboxyfluorescein (5'-6-FAM_40bp) was annealed at 10 μM concentration in annealing buffer (1X TE + 50 mM NaCl + 1 mM $MgCl_2$) with specific unlabeled oligos (sequences below) as follows: ssDNA (5'-6-FAM_40bp alone); dsDNA (5'-6-FAM_40bp + 40bp_for_ds); 5'-overhang (5'-6-FAM_40bp + 20bp_for_free5'); 3'-overhang (5'-6-FAM_40bp + 20bp_for_free3'); HJ (5'-6-FAM_40bp + HJ_strand2 + HJ_strand3 + HJ_strand4). Annealing was performed in a PCR machine using a temperature gradient from 95°C to 4°C, at a speed of 0.1°C per second. The EMSA reaction with 40-bp dsDNA or free 5' overhang were prepared (buffer contained 20 mM Tris-HCl pH 8.0, 1 mM DTT, 5 mM MgCl2, 5% glycerol) by keeping the DNA concentration constant and varying the protein concentration. After 10 min incubation and addition of 5% (w/v) sucrose, free DNA and DNA–protein complexes were resolved by electrophoresis on 6% TBE-acrylamide gels pre-equilibrated (pre-run for 30 min at 150 V) with running buffer (0.2X TBE buffer). Gels were run for 40 min at 100V at 4°C. Gels were imaged using a Bio-Rad ChemiDoc system using filters to image Cy2 dye. Gel bands were quantified using ImageJ (https://imagej.net), and binding curves were calculated using GraphPad Prism (https://www.graphpad.com) using a single-site binding model.

Oligonucleotide sequences:

5'_6-FAM_40bp : 6-FAM-CCTTTCGAAGACTCATCACGGAGAGCAGACATCATCTGGC

40bp_for_ds : GCCAGATGATGTCTGCTCTCCGTGATGAGTCTTCGAAAGG

20bp_for_free5': GCCAGATGATGTCTGCTCTC

20bp_for_free3': CGTGATGAGTCTTCGAAAGG

HJ_strand2: ATATATGATTCTAATAAGATCGTGATGAGTCTTCGAAAGG

HJ_strand3: GCCAGATGATGTCTGCTCTCGTCGTAATGTAAGTGTATGC

HJ_strand4: GCATACACTTACATTACGACATCTTATTAGAATCATATAT

Crystallographic data availability

Original diffraction data have been deposited with the SBGrid Data Bank (https://data.sbgrid.org) under accession numbers 538 (Zip2$^{499-704}$:Spo16 Form 1 Native), 539 (Zip2$^{499-704}$SER:Spo16 Form 2 Native), and 540 (Zip2$^{499-704}$SER:Spo16 Form 2, selenomethionine-derivatized SAD dataset). Reduced data and refined structures have been deposited with the RCSB Protein Data Bank (https://www.rcsb.org) under accession numbers 6BZF (Zip2$^{499-704}$:Spo16 Form 1) and 6BZG (Zip2$^{499-704}$SER:Spo16 Form 2).

Acknowledgements

The authors thank the staff of NE-CAT sector 24 beamlines at the Advanced Photon Source for assistance with data collection, processing, and phasing; and members of the Corbett lab for helpful discussions. This work was supported by NIH/NIGMS grant number R01GM104141.

Author Contributions

K.A. and K.D.C. designed the study. K.A. purified proteins determined x-ray crystal structures, and performed DNA binding assays. K.A. and K.D.C. wrote the manuscript.

Conflict of Interest

The authors declare no competing interests.

Figures

Figure 1. Zip2, Zip4, and Spo16 form a complex.

(A) Domain structure of Zip2, Zip4, and Spo16. Gray arrows indicate interactions identified by yeast two-hybrid and yeast three-hybrid analysis. The N-terminal domain of Zip2 has been proposed to contain a WD40 β-propeller domain (Perry *et al*, 2005), but modern structure-prediction algorithms do not support this assignment. HhH: helix-hairpin-helix, HhH_2: tandem helix-hairpin-helix. (B) Yeast two-hybrid analysis of interactions between Zip2, Zip4, and Spo16. See **Figure S1** for non-selective control plate. (C) Yeast three-hybrid analysis. See **Figure S1** for non-selective control plate. (D) Size exclusion chromatography/multi-angle light scattering (SEC-MALS) analysis of purified $Zip2^{499-704}$:Spo16. The measured molecular weight (51.8 kDa) is consistent with a 1:1 heterodimer (molecular weight 49.8 kDa). (E) SDS-PAGE analysis of purified $Zip2^{499-704}$:Spo16.

Figure 2. Structure of the $Zip2^{499-704}$:Spo16 complex.

(A) Domain schematic of Zip2 and Spo16 (top) and overall structure of the $Zip2^{499-704}$:Spo16 dimer. See **Figure S2** for an overlay of the five crystallographically-independent views of the dimer, and **Figure S3** for secondary-structure diagrams of both subunits. (B) Overlay of the Zip2 HhH_2 and Spo16 HhH domains. Cα r.m.s.d.= 2.65 Å over 34 atom pairs. HhH #1 comprises helices α and β separated by hairpin 1 (h1), and HhH #2 (not shared by Spo16) comprises helices δ and ε, separated by hairpin 2(h2). (C) Overlay of the Zip2 HhH_2 domain (pink) with the HhH_2 domain of *H. sapiens* XPF (PDB ID 1Z00; gray). Cα r.m.s.d.= 1.97 Å over 51 atom pairs. (D) Overlay of the Zip2 central domain (blue) with the *Aeropyrum pernix* XPF nuclease domain (gray) (PDB ID 2BGW) (Newman *et al*, 2005). Cα r.m.s.d.= 2.50 Å over 107 atom pairs. *Left:* close-up of the active site of *Ap* XPF (gray, with bound Mg^{2+} ion shown as a sphere) with the equivalent region of the Zip2 central domain (blue).

Figure 3. DNA binding by $Zip2^{499-704}$:Spo16.

(A-D) Representative gel-shift (*upper*) and binding curve from triplicate experiments (*lower*) for $Zip2^{499-704}$:Spo16 binding dsDNA (A), 5'-overhang (B), 3'-overhang (C), (D) and Holliday Junction DNA. Protein concentrations in each lane (left to right: 0, 0.625, 2.5, 5, 10, 20, and 40 μM) are the same for all gels. See **Figure S4A** for $Zip2^{499-704}$:Spo16 binding to ssDNA. (E) Surface charge distribution of the $Zip2^{499-704}$:Spo16 complex. The most highly positively-charged surface is located at the interface between the Zip2 central and HhH_2 domains. (F) Location of the putative DNA-binding surface of Zip2, with close-up (right) showing residues mutated in Zip2 DNA-binding mutants: mutant #1 (K663/K683/K686), mutant #2 (K609/K663/K683/K686). (G) Representative gel-shifts from $Zip2^{499-704}$:Spo16 DNA-binding mutant

#1 (K663A/K683A/K686A) binding to 5'-overhang and Holliday Junction DNA. (H) Representative gel-shifts from Zip2$^{499-704}$:Spo16 DNA-binding mutant #2 (R609A/K663A/K683A/K686A) binding to 5'-overhang and Holliday Junction DNA. See **Figure S4B, C** for analysis of DNA binding mutant #2 complex formation and stability.

Figure 4. Model for the role of Zip2:Spo14:Zip4 in meiotic crossover formation.

(A) Closeup view equivalent to **Figure 3F** of the putative DNA-binding surface of Zip2 (white with putative DNA-binding residues shown as sticks), with the structure of ssDNA-bound human XPF HhH_2 domain (PDB ID 2KN7) (Das *et al*, 2012) in yellow. Shown as sticks are three residues of the bound ssDNA; the remainder clash with the Zip2 central domain in our crystal structure. A potential path for DNA is shown as a thick yellow line, passing Zip2 R609. (B) Overall view of potential ssDNA-dsDNA junction (5' overhang) binding by Zip2$^{499-704}$:Spo16, based on the structural overlay in panel (A). A junction with this polarity is found in the D-loop recombination intermediate (gray arrow). (C) Model for the function of Zip2:Zip4:Spo16 in meiotic recombination. Initial strand invasion is mediated by Rad51 and Dmc1, and is continually counteracted by the dissolution activities of Sgs1, Top3, and Rmi1, resulting in SDSA. Recognition of specific DNA structures by Msh4:Msh5 (pro-HJ) and Zip2:Spo16 (ssDNA/dsDNA junction or pro-HJ) stabilize the strand-invasion/D-loop intermediate, recruit Type 1 CO-specific factors to promote the crossover outcome, and license assembly of the synaptonemal complex. Non-specific resolution of dHJs by Mus81-Mms4 or Yen1 (De Muyt *et al*, 2012) results in either NCO or Type 2 CO formation.

Supplemental Figures

Figure S1. Reductive alkylation and crystal packing in the Zip2$^{499-704}$:Spo16 Form 1 crystals.

(A) Schematic for reductive methylation of surface lysine residues by formaldehyde. (B) Representative electron density (F_o-F_c map contoured at 3.0 σ, calculated from a model missing the modified residue) for two dimethyl-lysine residues. (C) Schematic for the formation of hydroxymethylcysteine by reaction of cysteine with formaldehyde. (D) Representative F_o-F_c omit electron density (3.0 σ) for Zip2 cysteine 521. Chain A shown; the modified cysteine residue is clearly identifiable in all four Zip2 monomers of Form 1 crystals. (E) View of crystal packing interactions mediated by the N-terminal His_6-tag on Spo16, which also contains a TEV protease cleavage site. Residues from the tag that are visible in electron density are highlighted in green.

Figure S2. Structure of Zip2$^{499-704}$:Spo16.

(A) Overlay of the five crystallographically-independent views of Zip2$^{499-704}$:Spo16. The four copies of the complex in crystal form 1 are shown colored as in Figure 2, and the single copy of Zip2$^{499-704}$ SER:Spo16 in crystal form 2 is shown in gray. Overall Cα r.m.s.d. for all five copies ranges from 0.3 to 1.4 Å.

Figure S3. Secondary structure of Zip2 and Spo16.

(A) Secondary structure of the Zip2 central domain (left) and HhH_2 domain (right), with each domain colored as a rainbow from N- to C-terminus. Zip2 adopts a canonical XPF-like fold in both domains. (B) Secondary structure of the Spo16 central domain (left) and HhH domain (right), with each domain colored as a rainbow from N- to C-terminus. The Spo16 central domain lacks the N-terminal region (including β-strands 1 and 2, and α-helix A) found in ERCC1 and its homologs like FAAP24, and shows an extended β3-β4 loop and two additional short α-helices not found in its homologs. The Spo16 C-terminal domain lacks the second helix-hairpin-helix motif comprising α-helices δ and ε.

Figure S4. DNA binding by the Zip2$^{499-704}$:Spo16 complex.

(A) Representative gel-shift and binding curve for Zip2$^{499-704}$:Spo16 binding single-stranded DNA. DNA-binding affinity was not calculated. (B) Size-exclusion chromatography profile for wild-type Zip2$^{499-704}$:Spo16 and DNA-binding mutant #2 (R609A/K663A/K683A/K686A). (C) Thermofluor melting-temperature measurement for wild-type Zip2$^{499-704}$:Spo16 and DNA-binding mutant #2 (R609A/K663A/K683A/K686A). The change in fluorescence per temperature step (average of three independent measurements) is graphed; the maximum value is taken as the melting temperature (47°C for wild-type, 45°C for DNA-binding mutant #2).

Figure S5. Identification of a putative protein-protein interaction surface on Spo16.

Overall (left) and close-up (right) views of the Zip2$^{499-704}$ complex, with a crystallographic symmetry-related α-helix from Zip2 shown in cyan. This α-helix packs against a conserved hydrophobic cavity comprising the C-terminal W704 residue of Zip2 and several residues in the Spo16 HhH domain. This interface is observed in Form 2 crystals and two of the four dimers in Form 1 crystals.

Table S1. Crystallographic data and refinement

	Zip2$^{499-704}$:Spo16 Form 1	**Zip2$^{499-704}$SER:Spo16 Native Form 2**	**Zip2$^{499-704}$SER:Spo16 Semet Form 2**
Data collection			
Synchrotron/Beamline	APS 24ID-E	APS 24ID-C	APS 24ID-C
Date collected	10/29/16	6/15/17	6/15/17
Resolution (Å)	100 - 2.29	100 - 2.13	100 - 2.38
Wavelength (Å)	0.9792	0.9792	0.9792
Space Group	C2	$P2_12_12_1$	$P2_12_12_1$
Unit Cell Dimensions (a, b, c) Å	169.40 63.59 199.04	50.25 96.21 101.44	51.90 96.96 101.18
Unit cell Angles (α,β,γ) °	90, 90.60, 90	90, 90, 90	90, 90, 90
I/σ (last shell)	11.1 (0.8)	5.2 (0.7)	10.3 (0.8)
[1]R_{sym} (last shell)	0.091 (1.080)	0.207 (2.074)	0.104 (1.465)
[2]R_{meas} (last shell)	0.108 (1.432)	0.228 (2.246)	0.099 (1.597)
[3]$CC_{1/2}$ (last shell)	0.997 (0.328)	0.987 (0.484)	0.995 (0.390)
Completeness (last shell) %	98.6 (93.3)	99.8 (99.9)	98.4 (99.2)
Anomalous completeness (last shell) %	-	-	89.5 (90.2)
Number of reflections	337136	178386	63789
unique	95052	28219	20719
Multiplicity (last shell)	3.5 (2.3)	6.3 (6.8)	3.1 (3.1)
Refinement			
Resolution (Å)	2.286	2.130	-
No. of reflections	94878	52319	-
working	90072	49609	-
free	4806	2710	-
[4]R_{work} (last shell) (%)	19.56 (36.49)	24.92 (37.11)	-
[4]R_{free} (last shell) (%)	24.98 (39.54)	27.04 (41.95)	-
Structure/Stereochemistry			
No. of atoms	13182	3322	-
solvent	224	74	-
ligand	0	29	-
r.m.s.d. bond lengths (Å)	0.008	0.002	-
r.m.s.d. bond angles (°)	0.873	0.394	-
[5]SBGrid Data Bank ID	538	539	540
[6]Protein Data Bank ID	6BZF	6BZG	-

[1]$R_{sym} = \sum\sum_j |I_j - \langle I \rangle| / \sum I_j$, where I_j is the intensity measurement for reflection j and $\langle I \rangle$ is the mean intensity for multiply recorded reflections.

[2]$R_{meas} = \sum_h [\sqrt{(n/(n-1))} \sum_j [I_{hj} - \langle I_h \rangle] / \sum_{hj} \langle I_h \rangle$

where I_{hj} is a single intensity measurement for reflection h, $\langle I_h \rangle$ is the average intensity measurement for multiply recorded reflections, and n is the number of observations of reflection h.

[3]$CC_{1/2}$ is the Pearson correlation coefficient between the average measured intensities of two randomly-assigned half-sets of the measurements of each unique reflection (Karplus & Diederichs, 2012). $CC_{1/2}$ is considered significant above a value of ~0.15.

[4]$R_{work, free} = \sum| |F_{obs}| - |F_{calc}| | / |F_{obs}|$, where the working and free *R*-factors are calculated using the working and free reflection sets, respectively.

[5]Diffraction data for each structure have been deposited with the SBGrid Data Bank (https://data.sbgrid.org) with the noted accession codes.

[6]Coordinates and structure factors for each structure have been deposited with the Protein Data Bank (http://www.pdb.org) with the noted accession codes.

References

Adams PD, Afonine PV, Bunkóczi G, Chen VB, Davis IW, Echols N, Headd JJ, Hung LW, Kapral GJ, Grosse-Kunstleve RW, McCoy AJ, Moriarty NW, Oeffner R, Read RJ, Richardson DC, Richardson JS, Terwilliger TC & Zwart PH (2010) PHENIX: a comprehensive Python-based system for macromolecular structure solution. *Acta Crystallogr D Biol Crystallogr* **66:** 213–221

Afonine PV, Grosse-Kunstleve RW, Echols N, Headd JJ, Moriarty NW, Mustyakimov M, Terwilliger TC, Urzhumtsev A, Zwart PH, Adams PDIUCr (2012) Towards automated crystallographic structure refinement with phenix.refine. *Acta Crystallogr D Biol Crystallogr* **68:** 352–367

Ahuja JS, Sandhu R, Mainpal R, Lawson C, Henley H, Hunt PA, Yanowitz JL & Börner GV (2017) Control of meiotic pairing and recombination by chromosomally tethered 26S proteasome. *Science* **355:** 408–411

Bateman R, Rauh D & Shokat KM (2007) Glutathione traps formaldehyde by formation of a bicyclo[4.4.1]undecane adduct. *Org. Biomol. Chem.* **5:** 3363–3367

Berchowitz LE & Copenhaver G (2010) Genetic Interference: Don't Stand So Close to Me. *Curr. Genom.* **11:** 91–102

Bishop DK, Park D, Xu L & Kleckner N (1992) DMC1: a meiosis-specific yeast homolog of E. coli recA required for recombination, synaptonemal complex formation, and cell cycle progression. *Cell* **69:** 439–456

Borner GV, Barot A & Kleckner N (2008) Yeast Pch2 promotes domainal axis organization, timely recombination progression, and arrest of defective recombinosomes during meiosis. *Proc. Natl. Acad. Sci. USA* **105:** 3327–3332

Börner GV, Kleckner N & Hunter N (2004) Crossover/noncrossover differentiation, synaptonemal complex formation, and regulatory surveillance at the leptotene/zygotene transition of meiosis. *Cell* **117:** 29–45

Carballo JA, Johnson AL, Sedgwick SG & Cha RS (2008) Phosphorylation of the axial element protein Hop1 by Mec1/Tel1 ensures meiotic interhomolog recombination. *Cell* **132:** 758–770

Chen C, Jomaa A, Ortega J & Alani EE (2014) Pch2 is a hexameric ring ATPase that remodels the chromosome axis protein Hop1. *Proc. Natl. Acad. Sci. USA* **111:** E44–53

Chen SY, Tsubouchi T, Rockmill B, Sandler JS, Richards DR, Vader G, Hochwagen A, Roeder GS & Fung JC (2008) Global analysis of the meiotic crossover landscape. *Dev Cell* **15:** 401–415

Chua PR & Roeder GS (1998) Zip2, a meiosis-specific protein required for the initiation of chromosome synapsis. *Cell* **93:** 349–359

Ciccia A, McDonald N & West SC (2008) Structural and functional relationships of the XPF/MUS81 family of proteins. *Annu Rev Biochem* **77:** 259–287

Cloud V, Chan Y-L, Grubb J, Budke B & Bishop DK (2012) Rad51 is an accessory factor for Dmc1-mediated joint molecule formation during meiosis. *Science* **337:** 1222–1225

Das D, Folkers GE, van Dijk M, Jaspers NGJ, Hoeijmakers JHJ, Kaptein R & Boelens R (2012) The structure of the XPF-ssDNA complex underscores the distinct roles of the XPF and ERCC1 helix-hairpin-helix domains in ss/ds DNA recognition. *Structure* **20:** 667–675

De Muyt A, Jessop L, Kolar E, Sourirajan A, Chen J, Dayani Y & Lichten M (2012) BLM helicase ortholog Sgs1 is a central regulator of meiotic recombination intermediate metabolism. *Mol Cell* **46:** 43–53

Dong H & Roeder GS (2000) Organization of the yeast Zip1 protein within the central region of the synaptonemal complex. *J Cell Biol* **148:** 417–426

Emsley P, Lohkamp B, Scott WG & Cowtan K (2010) Features and development of Coot. *Acta Crystallogr D Biol Crystallogr* **66:** 486–501

Fung JC, Rockmill B, Odell M & Roeder GS (2004) Imposition of crossover interference through the nonrandom distribution of synapsis initiation complexes. *Cell* **116:** 795–802

Gibson DG, Young L, Chuang R-Y, Venter JC, Hutchison CA & Smith HO (2009) Enzymatic assembly of DNA molecules up to several hundred kilobases. *Nat Methods* **6:** 343–345

Goldschmidt L, Cooper DR, Derewenda ZS & Eisenberg D (2007) Toward rational protein crystallization: A Web server for the design of crystallizable protein variants. *Protein Sci* **16:** 1569–1576

Hassold T, Hall H & Hunt P (2007) The origin of human aneuploidy: where we have been, where we are going. *Human Molecular Genetics* **16 Spec No. 2:** R203–8

Hassold TJ & Hunt PA (2001) To err (meiotically) is human: the genesis of human aneuploidy. *Nat Rev Genet* **2:** 280–291

Hunter N & Kleckner N (2001) The single-end invasion: an asymmetric intermediate at the double-strand break to double-holliday junction transition of meiotic recombination. *Cell* **106:** 59–70

Joshi N, Barot A, Jamison C & Börner GV (2009) Pch2 links chromosome axis remodeling at future crossover sites and crossover distribution during yeast meiosis. *PLoS Genet* **5:** e1000557

Jurrus E, Engel D, Star K, Monson K, Brandi J, Felberg LE, Brookes DH, Wilson L, Chen J, Liles K, Chun M, Li P, Gohara DW, Dolinsky T, Konecny R, Koes DR, Nielsen JE, Head-Gordon T, Geng W, Krasny R, et al (2018) Improvements to the APBS biomolecular solvation software suite. *Protein Sci* **27:** 112–128

Kabsch W (2010) XDS. *Acta Crystallogr D Biol Crystallogr* **66:** 125–132

Karplus PA & Diederichs K (2012) Linking crystallographic model and data quality. *Science* **336:** 1030–1033

Kim Y, Quartey P, Li H, Volkart L, Hatzos C, Chang C, Nocek B, Cuff M, Osipiuk J, Tan K, Fan Y, Bigelow L, Maltseva N, Wu R, Borovilos M, Duggan E, Zhou M, Binkowski TA, Zhang R-G & Joachimiak A (2008) Large-scale evaluation of protein reductive methylation for improving protein crystallization. *Nat Methods* **5:** 853–854

Lynn A, Soucek R & Börner GV (2007) ZMM proteins during meiosis: crossover artists at work. *Chromosome Res* **15:** 591–605

Macaisne N, Novatchkova M, Peirera L, Vezon D, Jolivet S, Froger N, Chelysheva L, Grelon M & Mercier R (2008) SHOC1, an XPF Endonuclease-Related Protein, Is Essential for the Formation of Class I Meiotic Crossovers. *Current Biology* **18:** 1432–1437

Macaisne N, Vignard J & Mercier R (2011) SHOC1 and PTD form an XPF-ERCC1-like complex that is required for formation of class I crossovers. *J Cell Sci* **124:** 2687–2691

Malavasic MJ & Elder RT (1990) Complementary transcripts from two genes necessary for normal meiosis in the yeast Saccharomyces cerevisiae. *Mol Cell Biol* **10:** 2809–2819

Mazina OM, Mazin AV, Nakagawa T, Kolodner RD & Kowalczykowski SC (2004) Saccharomyces cerevisiae Mer3 helicase stimulates 3'-5' heteroduplex extension by Rad51; implications for crossover control in meiotic recombination. *Cell* **117:** 47–56

McCoy AJ, Grosse-Kunstleve RW, Adams PD, Winn MD, Storoni LC & Read RJ (2007) Phaser crystallographic software. *J Appl Crystallogr* **40:** 658–674

Metz B, Kersten GFA, Hoogerhout P, Brugghe HF, Timmermans HAM, de Jong A, Meiring H, Hove ten J, Hennink WE, Crommelin DJA & Jiskoot W (2004) Identification of formaldehyde-induced modifications in proteins: reactions with model peptides. *J Biol Chem* **279:** 6235–6243

Newman M, Murray-Rust J, Lally J, Rudolf J, Fadden A, Knowles PP, White MF & McDonald NQ (2005) Structure of an XPF endonuclease with and without DNA suggests a model for substrate recognition. *EMBO J* **24:** 895–905

Niu H, Li X, Job E, Park C, Moazed D, Gygi SP & Hollingsworth NM (2007) Mek1 kinase is regulated to suppress double-strand break repair between sister chromatids during budding yeast meiosis. *Mol Cell Biol* **27:** 5456–5467

Niu H, Wan L, Baumgartner B, Schaefer D, Loidl J & Hollingsworth NM (2005) Partner choice during meiosis is regulated by Hop1-promoted dimerization of Mek1. *Mol Biol Cell* **16:** 5804–5818

Niu H, Wan L, Busygina V, Kwon Y, Allen JA, Li X, Kunz RC, Kubota K, Wang B, Sung P, Shokat KM, Gygi SP & Hollingsworth NM (2009) Regulation of meiotic recombination via Mek1-mediated Rad54 phosphorylation. *Mol Cell* **36:** 393–404

Pape T, Schneider TRIUCr (2004) HKL2MAP: a graphical user interface for macromolecular phasing with SHELX programs. *J Appl Crystallogr* **37:** 843–844

Perry J, Kleckner N & Börner GV (2005) Bioinformatic analyses implicate the collaborating meiotic crossover/chiasma proteins Zip2, Zip3, and Spo22/Zip4 in ubiquitin labeling. *Proc Natl Acad Sci USA* **102:** 17594–17599

Rao HBDP, Qiao H, Bhatt SK, Bailey LRJ, Tran HD, Bourne SL, Qiu W, Deshpande A, Sharma AN, Beebout CJ, Pezza RJ & Hunter N (2017) A SUMO-ubiquitin relay recruits proteasomes to chromosome axes to regulate meiotic recombination. *Science* **355:** 403–407

Schwacha A & Kleckner N (1995) Identification of double Holliday junctions as intermediates in meiotic recombination. *Cell* **83:** 783–791

Schwacha A & Kleckner N (1997) Interhomolog bias during meiotic recombination: meiotic functions promote a highly differentiated interhomolog-only pathway. *Cell* **90:** 1123–1135

Sheldrick GM (2010) Experimental phasing with SHELXC/D/E: combining chain tracing with density modification. *Acta Crystallogr D Biol Crystallogr* **66:** 479–485

Shinohara M, Oh SD, Hunter N & Shinohara A (2008) Crossover assurance and crossover interference are distinctly regulated by the ZMM proteins during yeast meiosis. *Nat Genet* **40:** 299–309

Snowden T, Acharya S, Butz C, Berardini M & Fishel R (2004) hMSH4-hMSH5 recognizes Holliday Junctions and forms a meiosis-specific sliding clamp that embraces homologous chromosomes. *Mol Cell* **15:** 437–451

Snowden T, Shim K-S, Schmutte C, Acharya S & Fishel R (2008) hMSH4-hMSH5 adenosine nucleotide processing and interactions with homologous recombination machinery. *J Biol Chem* **283:** 145–154

Subramanian VV, Macqueen AJ, Vader G, Shinohara M, Sanchez A, Borde V, Shinohara A & Hochwagen A (2016) Chromosome Synapsis Alleviates Mek1-Dependent Suppression of Meiotic DNA Repair. *PLoS Biol* **14:** e1002369

Sym M, Engebrecht JA & Roeder GS (1993) ZIP1 is a synaptonemal complex protein required for meiotic chromosome synapsis. *Cell* **72:** 365–378

Terwilliger TC (2000) Maximum-likelihood density modification. *Acta Crystallogr D Biol Crystallogr* **56:** 965–972

Terwilliger TC (2003) Automated main-chain model building by template matching and iterative fragment extension. *Acta Crystallogr D Biol Crystallogr* **59:** 38–44

Terwilliger TC, Adams PD, Read RJ, McCoy AJ, Moriarty NW, Grosse-Kunstleve RW, Afonine PV, Zwart PH, Hung LWIUCr (2009) Decision-making in structure solution using Bayesian estimates of map quality: the PHENIX AutoSol wizard. *Acta Crystallogr D Biol Crystallogr* **65:** 582–601

Tsubouchi T, Zhao H & Roeder GS (2006) The meiosis-specific zip4 protein regulates crossover distribution by promoting synaptonemal complex formation together with zip2. *Dev Cell* **10:** 809–819

Walter TS, Meier C, Assenberg R, Au K-F, Ren J, Verma A, Nettleship JE, Owens RJ, Stuart DI & Grimes JM (2006) Lysine methylation as a routine rescue strategy for protein crystallization. *Structure* **14:** 1617–1622

Wang S, Zickler D, Kleckner N & Zhang L (2015) Meiotic crossover patterns: obligatory crossover, interference and homeostasis in a single process. *Cell Cycle* **14:** 305–314

Winn MD, Ballard CC, Cowtan KD, Dodson EJ, Emsley P, Evans PR, Keegan RM, Krissinel EB, Leslie AGW, McCoy A, McNicholas SJ, Murshudov GN, Pannu NS, Potterton EA, Powell HR, Read RJ, Vagin A & Wilson KS (2011) Overview of the CCP4 suite and current developments. *Acta Crystallogr D Biol Crystallogr* **67:** 235–242

Yang H, Zhang T, Tao Y, Wang F, Tong L & Ding J (2013) Structural insights into the functions of the FANCM-FAAP24 complex in DNA repair. *Nucleic Acids Res* **41:** 10573–10583

Zakharyevich K, Tang S, Ma Y & Hunter N (2012) Delineation of joint molecule resolution pathways in meiosis identifies a crossover-specific resolvase. *Cell* **149:** 334–347

Zickler D & Kleckner N (1999) Meiotic chromosomes: integrating structure and function. *Annu Rev Genet* **33:** 603–754

Figure 1

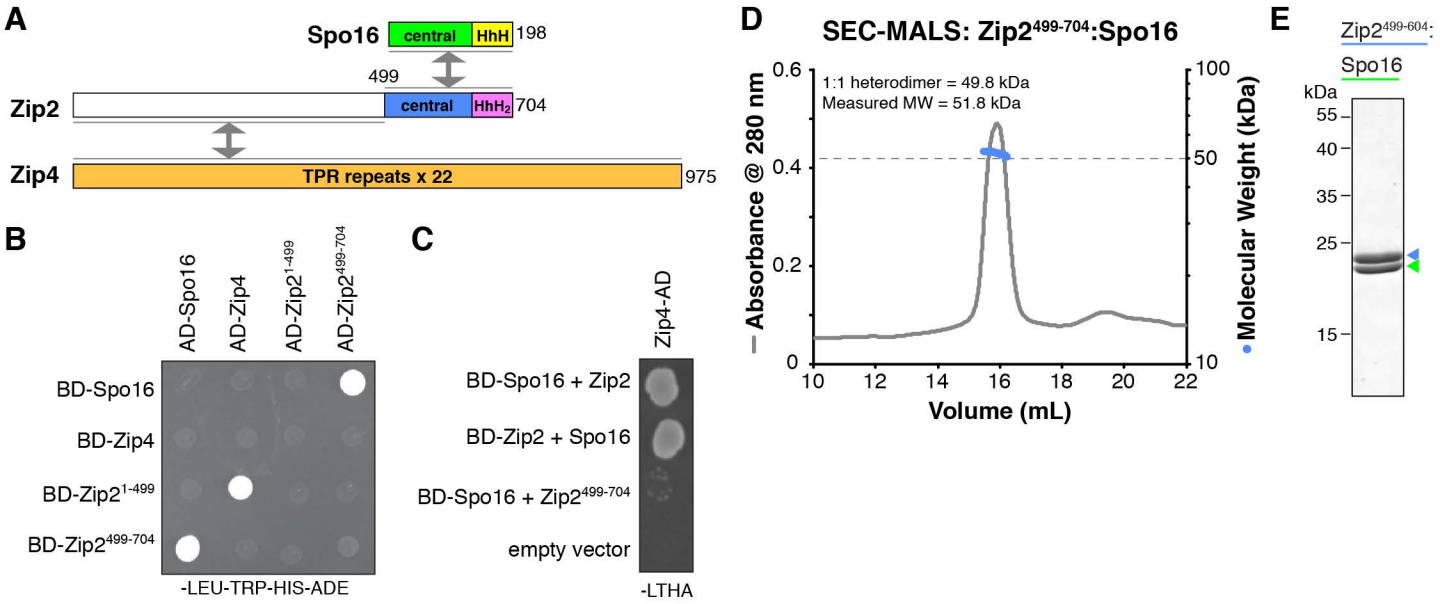

Figure 2

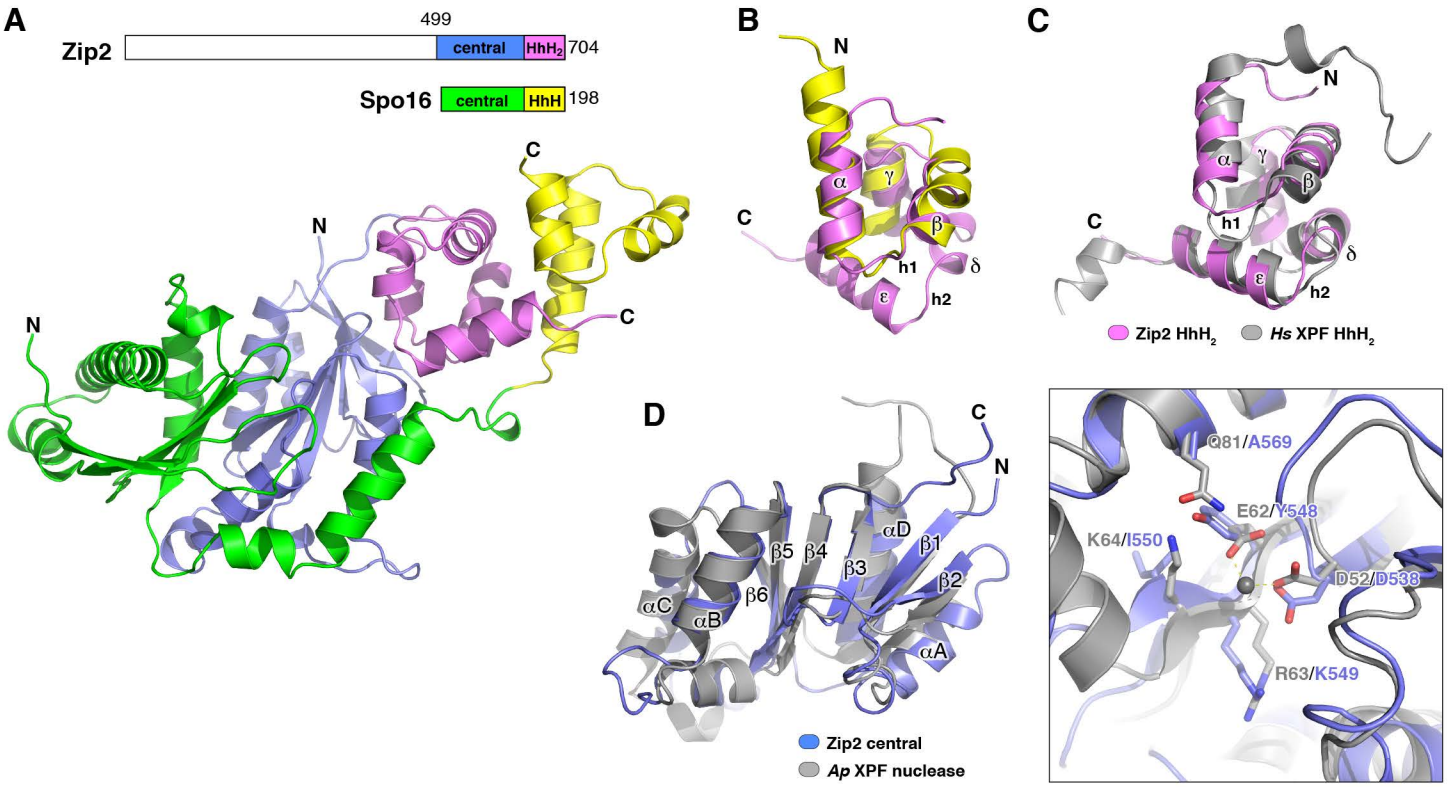

Figure 3

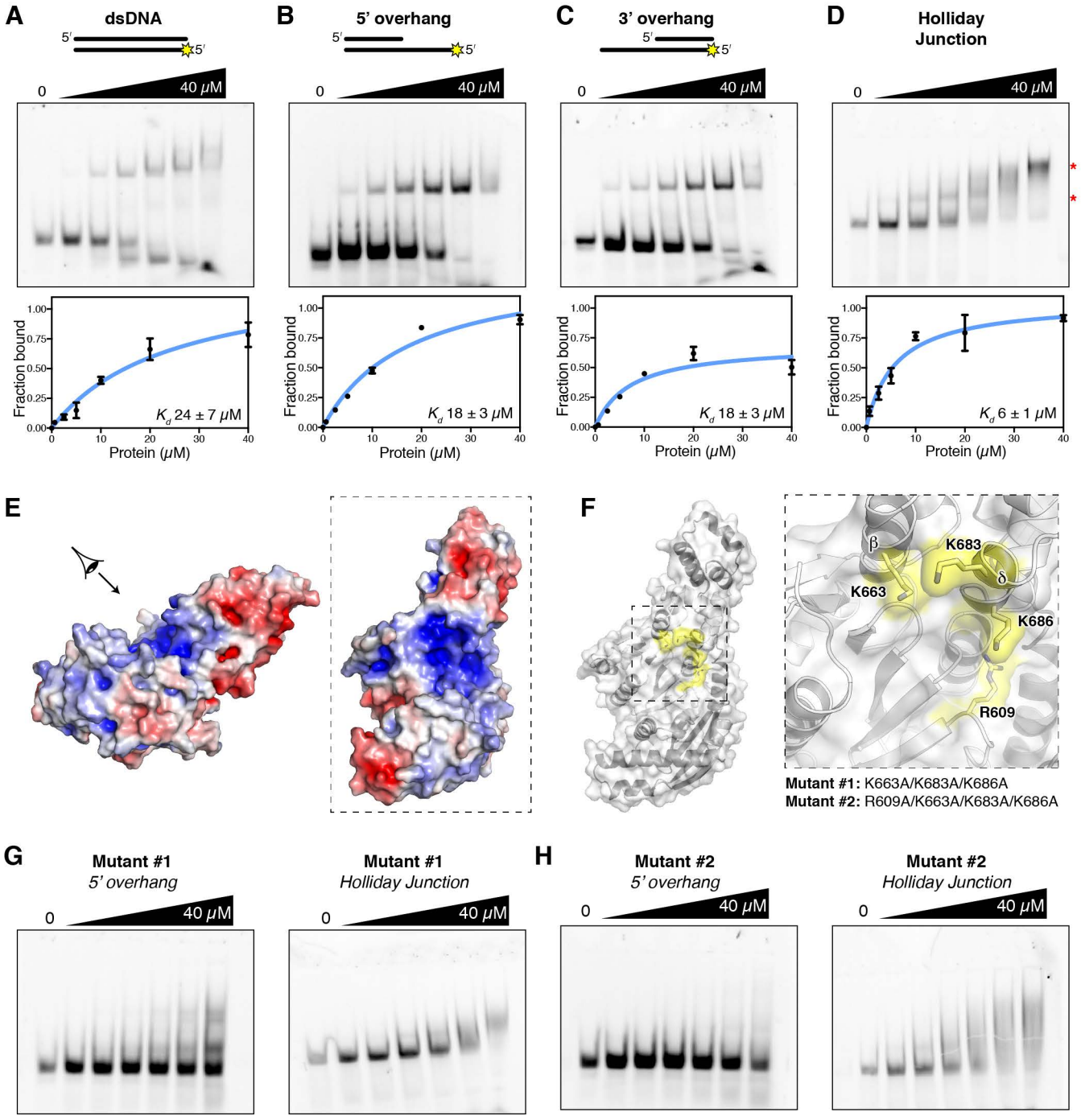

Figure 4

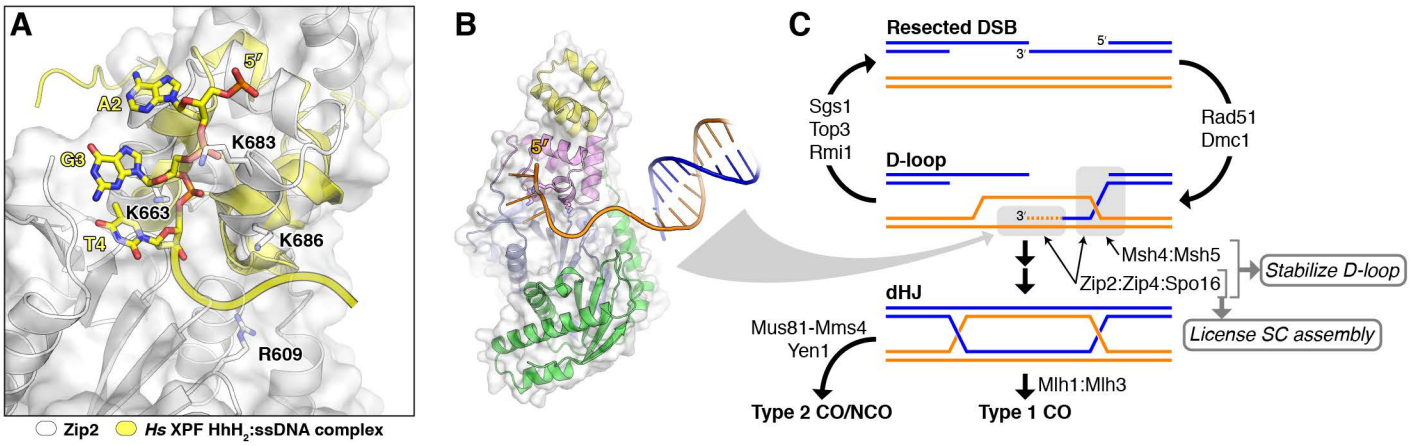

Figure S1

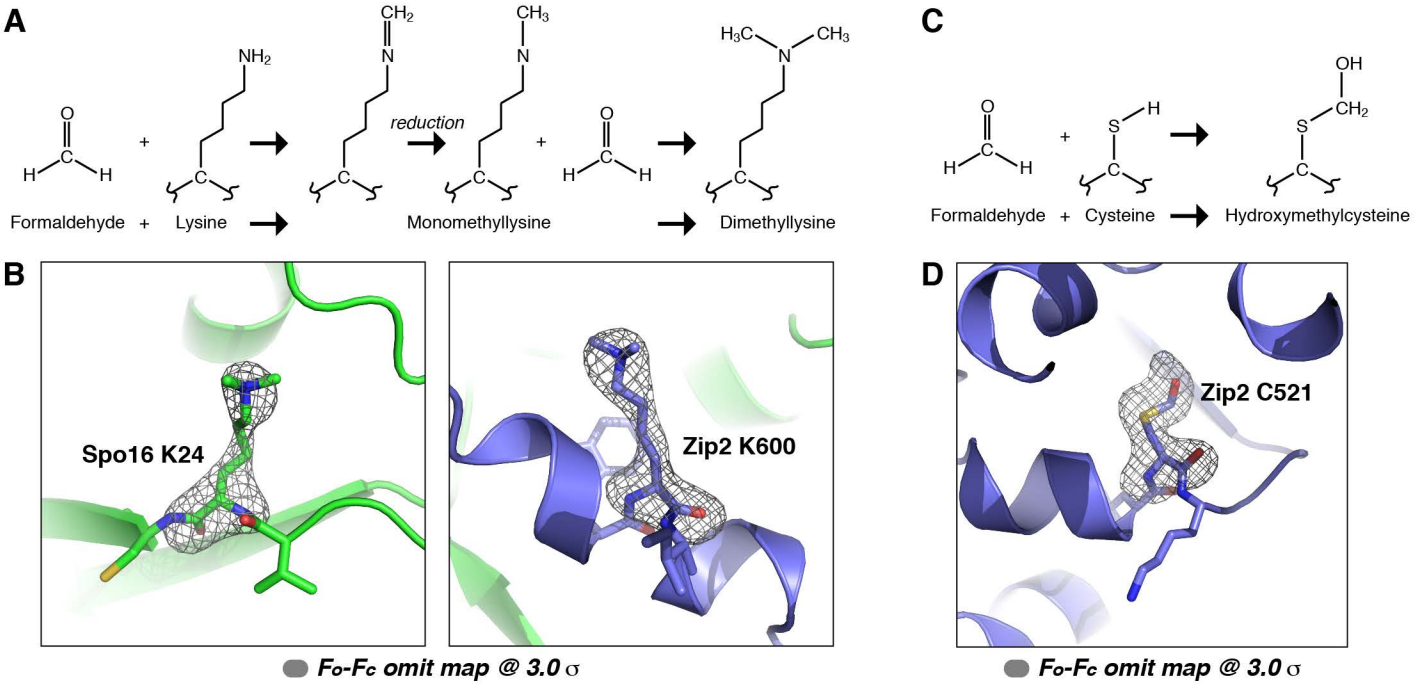

MKSSHHHHHHENLYFQ^SNA-[Spo16$^{2\text{-}198}$]

Figure S2

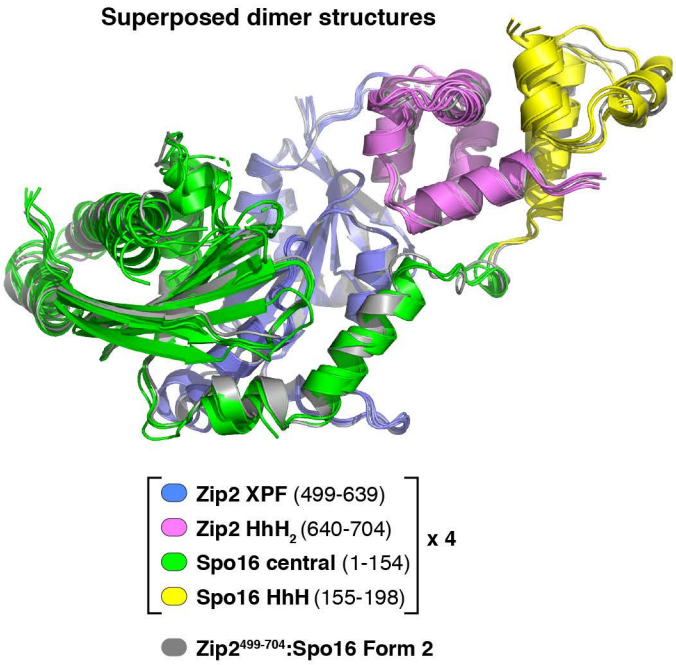

Figure S3

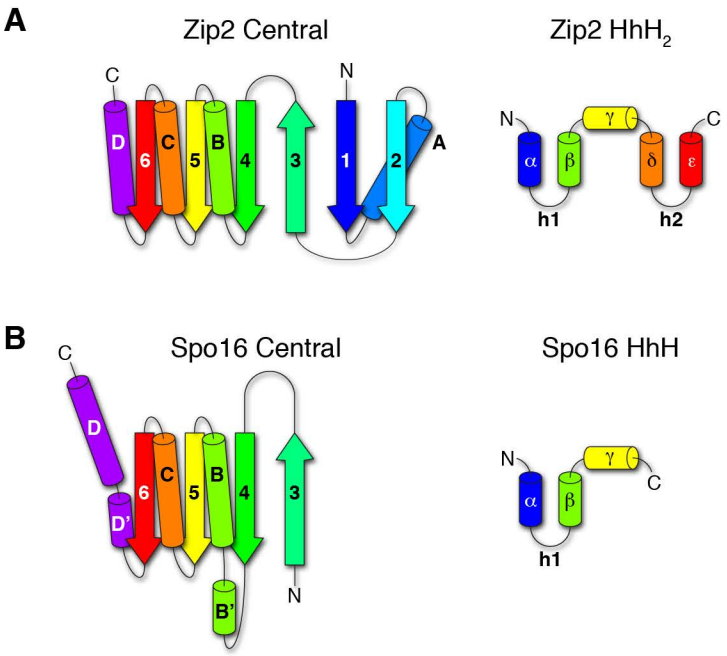

Figure S4

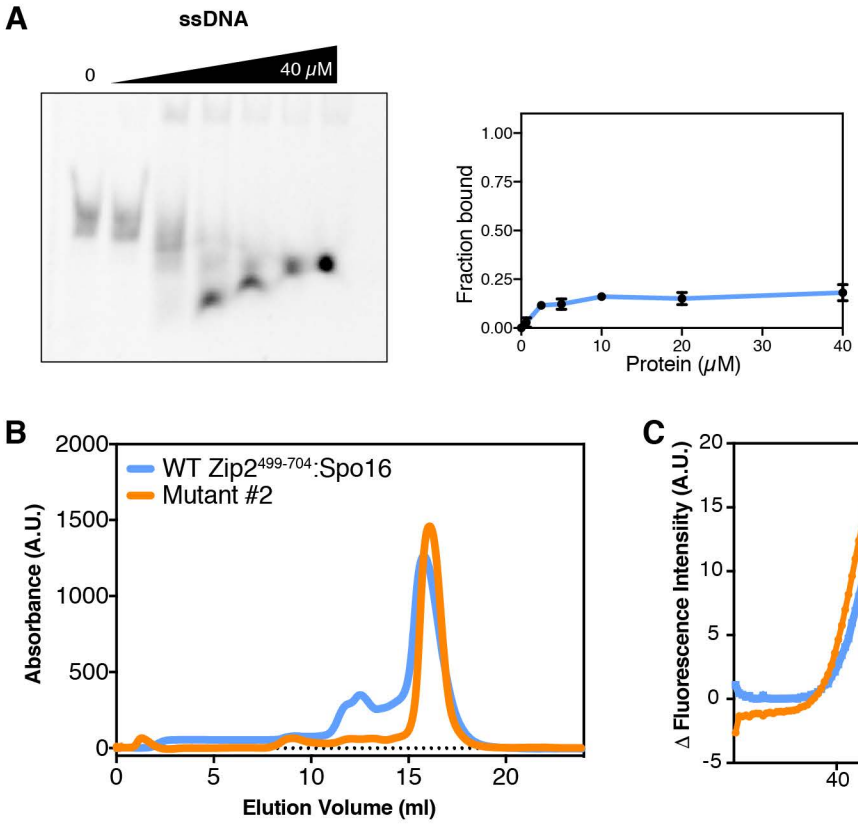

Figure S5